One Step Creation of Multifunctional 3D Architectured Hydrogels Inducing Bone Regeneration

*Axel T. Neffe, Benjamin F. Pierce, Giuseppe Tronci, Nan Ma, Erik Pittermann, Tim Gebauer, Oliver Frank, Michael Schossig, Xun Xu, Bettina M. Willie, Michèle Forner, Agnes Ellinghaus, Jasmin Lienau, Georg N. Duda, and Andreas Lendlein**

Critical size defects in bone,[1] which do not heal by themselves, occur after trauma, infection, or tumor resections.[2] Rising awareness of the socioeconomic impact and the lack of adequate treatments have stimulated significant scientific attention on creating therapeutic options for bone regeneration.[3] Inducing and controlling bone regeneration is widely thought to be ruled by applying soluble bioactive factors or multipotent cells.[4] Biomaterials have been applied successfully as supportive means for controlled factor release[5] or for providing a temporary extracellular matrix (ECM) substitute to cells in tissue engineering approaches.[6] In comparative studies, degradable biomaterials by themselves as a pure biomaterial approach did not lead to satisfying regeneration.[5a,7] Such an in situ tissue regeneration would require homing of residual cells and potentially influence stem cell differentiation,[8] which has generally been supported through specific peptides or growth factors.[9] Therefore, cancellous bone grafts are still the clinical standard,[10] which are associated with limited availability, donor site morbidity, and inflammatory risks.[11]

Here, we aim at a cell- and factor-free, purely biomaterial-induced regeneration[12] with a 3D architectured hydrogel (ArcGel) consisting of gelatin and lysine connected by urea junction units. We hypothesize that such a structured hydrogel can be equipped with multiple functions to guide tissue regeneration by providing a microenvironment enabling homing of cells as well as inducing osteogenic differentiation and tissue formation, which is supported by a fast and spatially directed degradation of the material. We introduce multifunctional ArcGels based on gelatin which can be prepared in a one-step process integrating the formation of an open porous morphology and the chemical functionalization, and which successfully induce regeneration of bone in vivo. Their key functions are cell adhesion support, tailorable microscopic (cell environment) and macroscopic elastic properties, as well as growing pores during the degradation period of a few weeks. These features provide an osteogenic environment.

Our biomaterial design combines three principles: i) An open porous interconnected structure allows rapid[6a,7b] cell invasion, which is supported by cell adhesion sites[13] and an elastic behavior of the material. This enabling of residual cells to migrate in vivo into the 3D ArcGels distinguishes our approach[14] fundamentally from cells which are encapsulated in gels before implantation[15] (**Figure 1**a). ii) An osteogenic environment will be provided by tailoring the elastic properties of the pore walls. This substrate elastically determined differentiation approach aims at transferring concepts from stroma cell research[15a,16] into void regeneration. Such mechanotransduction again requires sufficient adhesion sites for cells on the material surface with a suitable spatial distribution (Figure 1b).[17] iii) Finally, fast degradation of the material with growing pore size guiding the tissue development shall be realized. Synthetic polyesters such as poly(glycolide-*co*-lactide) (PLGA) and poly(ε-caprolactone) do not degrade in the time frame of callus formation (six weeks). But with biopolymers, this degradation time period can be achieved because of rapid enzymatic degradation. The growth of pores during degradation corresponds to the demands in biomaterial-induced endogenous regeneration, in which initially small pores lead to better adhesion of cells,[18] while cell ingrowth, angiogenesis, and tissue formation is profiting from larger pores, higher surface areas, and greater interconnectivity at a later stage of the regeneration.[19]

The preparation of a biomaterial combining these different functions in a single step process represents a scientific

Dr. A. T. Neffe, Dr. B. F. Pierce, Dr. G. Tronci,[+]
Prof. N. Ma, T. Gebauer, O. Frank,
M. Schossig, X. Xu, Prof. A. Lendlein
Institute of Biomaterial Science
Helmholtz-Zentrum Geesthacht
Kantstrasse 55, 14513 Teltow, Germany
E-mail: andreas.lendlein@hzg.de

Dr. A. T. Neffe, Dr. B. F. Pierce, Prof. N. Ma, Dr. J. Lienau,
Prof. G. N. Duda, Prof. A. Lendlein
Berlin-Brandenburg Center for Regenerative Therapies
Augustenburger Platz 1
13533 Berlin and Kantstr. 55, 14513 Teltow, Germany

Prof. N. Ma
Institute of Chemistry and Biochemistry
Freie Universität Berlin
Takustr. 3, 14195 Berlin, Germany

E. Pittermann
Clinic for Heart Surgery
FKGO Laboratory
University of Rostock
Schillingallee 35, 18057 Rostock, Germany

Dr. B. M. Willie, Dr. M. Forner, Dr. A. Ellinghaus,
Dr. J. Lienau, Prof. G. N. Duda
Julius Wolff Institute and Center for Musculoskeletal Surgery
Charité-Universitätsmedizin Berlin
Augustenburger Platz 1, 13533 Berlin, Germany

[+]Present address: School of Dentistry, University of Leeds, UK

DOI: 10.1002/adma.201404787

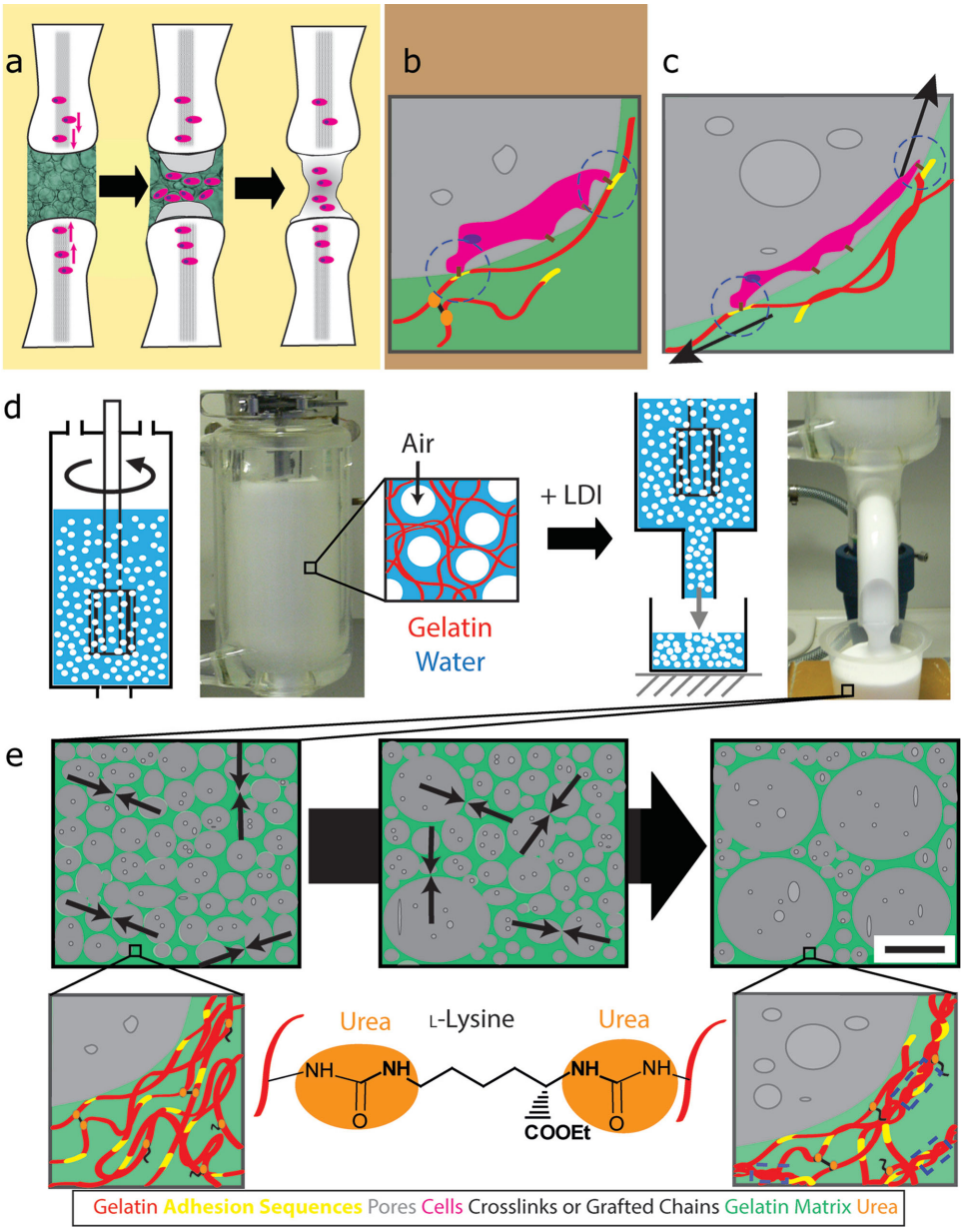

Figure 1. a) Strategy for gelatin-based 3D architectured hydrogels (ArcGels) induced bone regeneration. The cell-free material is implanted, cells invade the ArcGel, and bone is regenerated. b) During cell settling, cells sense the elasticity of the matrix through contact with adhesion sites. c) During degradation, contact to adhesion sites and pore growth lead to mechanical stimulation of the cells. d) Foams are generated from an aqueous solution of gelatin and a PEG–PPG–PEG triblock copolymer as surfactant at 45 °C through stirring. Stabilization of the ArcGels was achieved by reaction with L-lysine diisocyanate ethyl ester (LDI). e) The resulting ArcGels have an open porous structure. Through hydrolytic degradation of walls (green) over time, the wall tension is released (indicated by arrows) to give pore (gray) growth during degradation (top). On the molecular level (bottom), the bulk of the material consists of gelatin chains (red), which are grafted with and crosslinked by lysines (black). The gelatin-inherent adhesion peptides (yellow) are partially presented on the ArcGel walls where they are accessible to cells and proteins. Degradation increases the mobility of gelatin chains enabling partial reheli-calization to collagen-like triple helices (highlighted in frames). The scale bar in the scheme is for orientation purposes only and represents ≈200 µm.

challenge.[20] Here, we present such a one-step approach for creating multifunctionality in a structured hydrogel system by integrating synthesis and formation. We have chosen gelatin as starting material as it provides adhesion sites for cells[21] and proteins, it is rapidly degradable, hydrogel forming, and readily available. We envisioned creating a porous structure similar to the process of whipping cream, simultaneously functionalizing gelatin with a derivative of the amino acid L-lysine via urea junction units. In this way, a material consisting only of protein chains and amino acid derivatives acting as crosslinkers is formed. The open porous structure results from the collapse of thin walls formed by air incorporation (Figure 1d). We speculate that through control of the crosslink density the local mechanical properties can be tailored, while the overall macroscopic

mechanical properties of the hydrogels are ruled additionally by the 3D architecture. The entropy elastic behavior of the network should result in growing pores of the structured hydrogel during the degradation process, like soap bubbles merging (Figure 1e). Interestingly, such features, together with the adhesion sites on the material, could lead to active mechanical stress on adhered proteins and cells (Figure 1c). The increased flexibility of the gelatin chains after hydrolysis of crosslinks allows for self-organization into triple helices, which should counteract the reduction of *E*-modulus generally observed in degradation processes of hydrogels.

In the following, the formation and characterization of the ArcGels are presented, followed by in vitro cell culture experiments in which attachment, growth, and differentiation of human mesenchymal stroma cells (hMSCs) in the ArcGels are shown, and finally the effectiveness of the cell-free ArcGels to induce bone formation in a critical size bone defect in a rat model will be described.

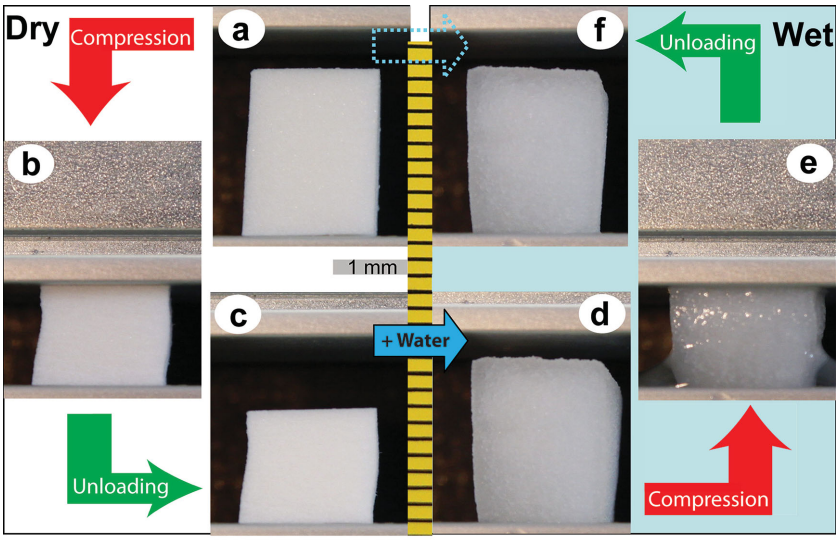

Figure 2. Macroscopic form upon compression, unloading, or wetting at ambient temperature shown exemplarily for G13_LNCO8. When a dry ArcGel (a) is compressed (b), it retains its shape when the load is removed (c) (plastic deformation). Addition of water leads to the recovery of the original shape (d) (water-induced shape-memory effect). When the wet ArcGel is compressed (e), it fully recovers elastically after removal of the load (f). The outer dimensions of the ArcGel do not change upon the addition of water and thus it is macroscopically form stable (a–f) (see Figure S2, Supporting Information). The cycle can be repeated several times. The elastic recovery is of relevance during the implantation procedure (compare with Figure 1a) The scale unit on the ruler is 1 mm.

The ArcGels were prepared with varying molar excess of L-lysine diisocyanate ethyl ester (LDI) compared to free amino groups of gelatin as well as gelatin concentration in the presence of a surfactant. They are referred to as G*X*_LNCO*Y*, in which *X* describes the gelatin concentration (wt%) and *Y* the molar excess of isocyanate groups. Although several competing reactions are observed, the reaction of gelatin with diisocyanates in aqueous solution in the presence of a surfactant gave a controlled number of lysine crosslinks and grafted oligolysine chains, with single or two units being predominant (for mechanism, see ref. [22]). For the investigated ratios of diisocyanate to amino groups of gelatin, the synthesis led to stable ArcGels (Figure 1b). In order to ensure this tailorability, it was essential to initially suppress the self-organization of gelatin chains in single and triple helices, which was accomplished by performing the reaction above the helix-coil-transition temperature. Wide-angle x-ray scattering (WAXS) studies of the ArcGels showed only low single-helical (1%) or triple-helical (1–2%) contents, which proved that this approach was successful (compare Figure S4, Supporting Information). All ArcGels featured an interconnected pore morphology, with the pore sizes of the synthesized ArcGels in the dry state ranging from 156 ± 56 to 286 ± 92 µm (determined by scanning electron microscopy (SEM) as well as microcomputed tomography (µCT)).[26] The ArcGels took up water (900–1100 wt% at room temperature), with lower water uptake observed for G13_LNCO8 than for the G10 samples. The water uptake properties of the scaffolds corresponded to their overall densities, which increased with increasing LDI amount added during the synthesis for the G10 ArcGels (66 ± 3 to 96 ± 3 mg cm^{-3}).

The ArcGels showed remarkable behavior in compression tests. Wet ArcGels elastically recovered after removal of external stress (**Figure 2**d–f), while dry ArcGels showed plastic deformation (Figure 2a–c), with a shape fixity ratio R_f of 85 ± 5% (G10_LNCO3) and 80 ± 5% (G10_LNCO8). When water was added to the compressed dry ArcGels, the original shapes of the ArcGels were recovered (Figure 2c,d), with a shape recovery ratio R_r of 88 ± 5% (G10_LNCO3) and 95 ± 5% (G10_LNCO8). This behavior corresponds to a water-induced shape-memory effect (SME)[23] in which the thermal transition temperature associated to the switching domains is decreased, while the environmental temperature remained constant. The addition of water reduces T_g of the ArcGels from 50–62 °C (dry) to below 0 °C (wet) as determined by dynamic mechanical analysis at varied temperature (DMTA). Despite the high water uptake, the macroscopic outer dimensions of the ArcGels did not significantly change during the wetting process, i.e., neither expansion nor shrinkage was observed. Thus, they were form stable (Figure 2a/f and the Supporting Information) in contrast to clinically applied collagen sponges (Lyostypt), which showed substantial shrinkage (41 vol%) upon contact with water and easily disintegrated when handled.

While the macroscopic properties of the ArcGels are important for handling, the cell–biomaterial interactions occur locally in the microenvironment. The pore sizes of the ArcGels in the wet state (192 ± 59 to 209 ± 54 µm) as determined using light microscopy did not differ from pore sizes in ArcGels in the dry state at room temperature. Only a small increase in wall thickness during water uptake was observed, which can be explained by the incorporation of water molecules into a large free volume of the ArcGels, which is likely resulting from the freeze-drying step. Pore dimensions and their microform stability imply that the ArcGels structure enable cell invasion and amplification.

It was demonstrated for stroma cells on 2D hydrogel substrates[16a,b] or enclosed in dense hydrogel matrices[15] that

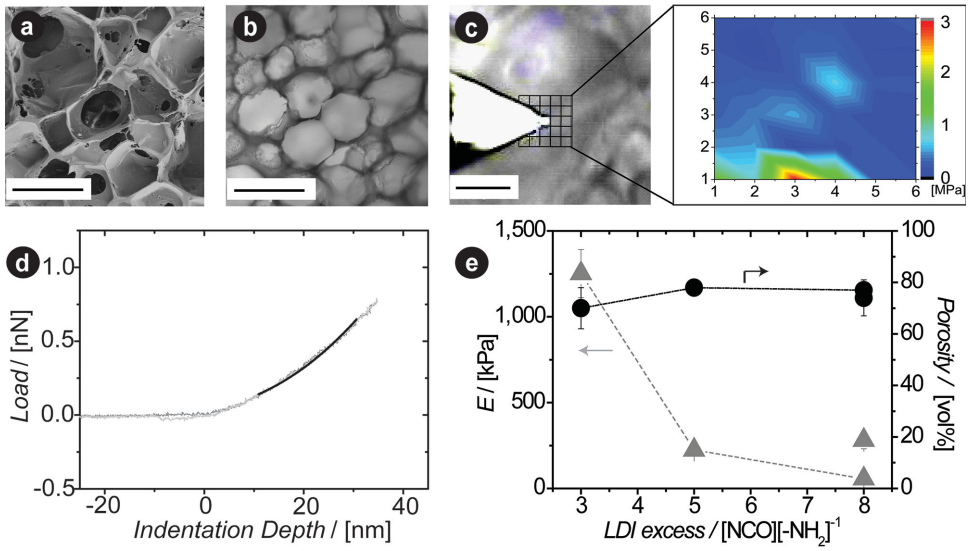

Figure 3. ArcGel porosity and micromechanical properties of the ArcGels' pore walls. a) Scanning electron microscopy image of the dry ArcGel G13_LNCO8. The scale bar represents 200 µm. b) Light microscopy image of the same ArcGel at a different position in the wet state, showing microscopic form stability (see Figure S3, Supporting Information, for details). The scale bar represents 200 µm. c) Optical microscopy-guided positioning of the AFM tip for the indentation experiments on this ArcGel. The grid shows the corresponding indentation area. Enlarged is the corresponding indentation map giving the local Young's moduli *E*. The scale bar represents 30 µm. d) Exemplary force–distance curve for AFM measurements of G10_LNCO5, with the theoretical fit highlighted in black. e) Porosity of dry G10_LNCOX ArcGels determined by µCT (●) and *E* of wet ArcGel walls determined by AFM (▲). The data points separated from the connected curves correspond to G13_LNCO8. Compare with Figure 1b.

they respond differently to substrates with varied macroscopic elastic moduli. Therefore, we hypothesized that the elastic modulus of the microenvironment is highly relevant to guide cell fate within the ArcGels. Determining the local micromechanical properties of the wet ArcGels was challenging from an experimental point of view as the heterogeneous, porous structure required precise positioning of the mechanical testing device to specifically indent on the pore walls and not the aqueous phase. We accomplished this by combining an optical microscope and an atomic force microscope (AFM). An area on an ArcGel surface was identified, which could be scanned with an AFM tip without the cantilever touching any protruding parts of the ArcGel. Therefore, the difference in profile height of the scanned area had to be smaller than the height of the AFM tip (3 µm). Such areas were identified by optical microscopy and confirmed by quantifying the surface roughness of this area. This was achieved by acquiring a force map (30 × 30 µm) identical to the studied area with the lowest possible trigger point of the cantilever, which corresponded to a middle indentation depth of 60–500 nm. Subsequently, force–distance curves were determined and the Young's moduli of single points were calculated by fitting a modified Hertz model (see the Supporting Information).

The local *E* moduli of the G10 series decreased from 1250 ± 140 to 56 ± 28 kPa with increasing LDI excess (three- to eightfold) added during the synthesis (**Figure 3**). With increasing diisocyanate excess, the probability for the formation of direct crosslinks ruling the mechanical properties is decreasing. In case of high diisocyanate concentrations, the free amino groups rapidly reacted with different diisocyanate molecules, guiding the reaction in an early stage into the direction of grafting.

The main factors contributing to the macroscopic compressive modulus are the hydrogel architecture, the modulus of the pore walls, and the material density. For the G10 samples, the morphology is constant, while the modulus decreases and the density increases with LDI excess. These opposing trends seem to compensate each other on the macroscopic level. Therefore, the local *E* modulus can be adjusted independently from the macroscopic compression modulus.

The ArcGels were designed to degrade so that they would act as a temporary microenvironment fostering the migration and osteogenic differentiation of cells, while at subsequent stages provide a guiding structure for tissue development, allowing more space for proliferating cells. The mechanisms of degradation were studied in vitro. The pore size changes during degradation, measured in freeze-dried ArcGels, were monitored with SEM and showed that average pore sizes of hydrolytically degrading ArcGels increased (as shown for G10_LNCO8 in **Figure 4**a). As hypothesized, pores merged during degradation, i.e., when a wall was degraded, the surface tension of the merged pore results in the formation of new, larger, round pores rather than tunnels (compare Figure 4 and 1). Despite the pores merging, the integrity of the ArcGels was retained for an unexpectedly long time period. This can be rationalized by the observation of a step-by-step self-organization of the peptide chains into single helices and triple helices as quantified from WAXS spectra (Figure 4). This potentially slows down the degradation and counteracts an undesired stronger swelling during degradation. G10_LNCO3 completely degraded after six weeks and G10_LNCO8 within ten weeks in in vitro studies, so the mass loss inversely correlated with the density.

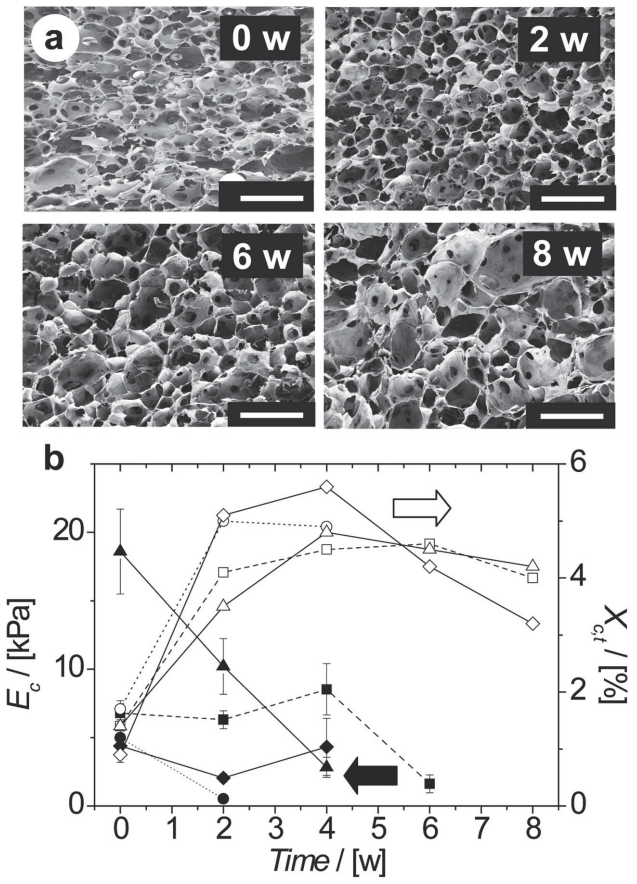

Figure 4. Hydrolytic degradation of ArcGels (PBS pH 7.4, 37 °C): a) SEM of freeze-dried ArcGel G10_LNCO8 initially and after 2, 6, and 8 weeks of degradation.The scale bars represent 200 µm each. b) Macroscopic compression modulus of the wet ArcGels (E_c, filled data points) and relative amount of triple helical contents ($X_{c,t}$, unfilled data points) as measured after freeze-drying of partially degraded ArcGels: (-●-) G10_LNCO3, (-■-) G10_LNCO5, (-◆-) G10_LNCO8, and (-▲-) G13_LNCO8. Compare to Figure 1c,e.

Altogether, the rate of degradation of the ArcGels is faster than generally suggested as appropriate for classical PLGA scaffolds intended for in vivo tissue engineering.[24] However, the importance of the early healing phase including cell migration and osteogenic differentiation for triggering and guiding regeneration cannot be overestimated and is targeted in our work.

The two ArcGels G10_LNCO3 and G10_LNCO8 were selected for further in vitro and in vivo analyses according to our hypothesis about the influence of micromechanical properties and degradation behavior to determine their potential to induce and guide bone regeneration. They differed only in micromechanical properties and rate of degradation, while keeping constant the macroscopic mechanics, pore sizes, and degree of helicity. In this way, the early effects on cell proliferation and differentiation should be ruled by the micromechanical properties of the ArcGels, while during subsequent stages of tissue development the effects of degradation will become more relevant. In a first step, ArcGels sterilized with ethylene oxide were tested for their cytocompatibility using L929 fibroblast cells according to the EN DIN ISO standard 10993-5 and showed noncytotoxic properties. Next, the viability and differentiation of hMSCs in the ArcGels was investigated in an in vitro spinner flask bioreactor (see the Supporting Information). Confocal microscopy examination and 3D reconstruction movies evidenced viable MSCs were homogenously distributed along both surface and interior of the ArcGels as early as 3 h after cell seeding. Overall, cell density in the ArcGels increased remarkably after 24 h (Figures S5 and S6, Supporting Information). At these early timepoints, the ArcGel cell invasion and viability was comparable in both ArcGel compositions.

After nine days of culture, hMSCs were homogeneously distributed in the ArcGels. They adhered to pore walls (**Figure 5**a), and no difference in viability was found in respect to the spatial location. A higher cell proliferation was observed on the softer

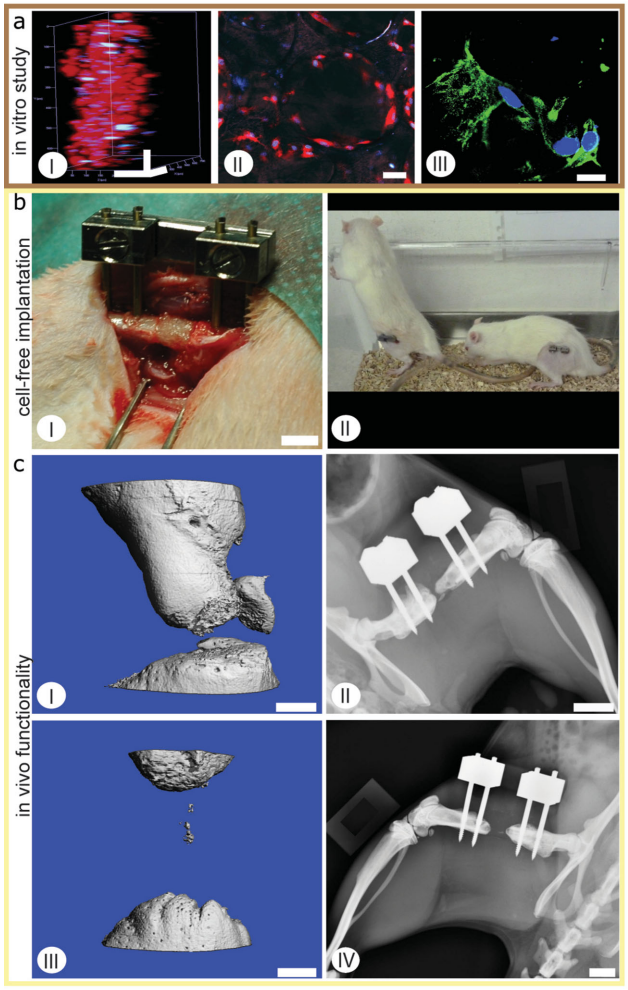

Figure 5. In vitro and in vivo performance of ArcGels G10_LNCO3 and G10_LNCO8. a) (I) The ArcGels (here exemplarily G10_LNCO3) supported proliferation of human bone marrow stem cells (hMSCs) in 3D cultures. (II) hMSCs adhere to the ArcGel walls and expand. (III) Differentiation along the osteogenic lineage was observed. Osteocalcin labeled in green, cell nuclei in blue, cytoplasm in red. b) Rats well tolerated (I) the implantation of cell-free ArcGels and (II) the external fixator. c) Postmortem µCT measurement representing new bone formation (left). X-ray of the critical defect after six weeks of implantation (right). I/II show G10_LNCO3, III/IV G10_LNCO8. Scale bars: a) I: 100, II: 50, III: 20 µm; b) I: 5 mm; c) I, III: 1, II, IV: 7 mm.

Table 1. Number of viable cells and differentiation of hMSCs in the ArcGels in vitro, and quantification of bone healing by μCT analysis (postmortem) of the fracture callus from rats after six weeks of healing.

	G10_LNC03	G10_LNC08	Cancellous bone graft
Number of viable cells	8020 ± 450[a)]	12 900 ± 3475[a)]	n.d.
	18 020 ± 1130[b,c)]	28 650 ± 1590[b,c)]	n.d.
Differentiation [%]	13.5 ± 3.3[a)]	n.o.	n.d.
	26.9 ± 4.5[b,c)]	8.8 ± 1.6[b,c)]	n.d.
TV[d,e,f)] [mm^3]	27.06 ± 10.84	11.07 ± 8.00	20.12 ± 11.98
BV[d,e,f)] [mm^3]	14.04 ± 7.15	6.16 ± 4.35	16.25 ± 9.42
BV/TV[d,e,f)] [mm^3/mm^3]	0.51 ± 0.14	0.56 ± 0.14	0.82 ± 0.06
TMD[d,e,f)] [mg HA cm^{-3}]	872 ± 64	825 ± 62	899 ± 51
TMC[d,e,f)] [mg]	12.24 ± 6.51	5.01 ± 3.46	14.43 ± 8.4

[a)]Uncoated; [b)]Fibronectin coated; [c)]Significantly different, unpaired t-test $p < 0.01$; [d)]TV: total callus volume, BV: mineralized callus volume, BV/TV mineralized callus volume fraction, TMD: tissue mineral density, TMC: tissue mineral content, HA: hydroxy apatite, n.d.: not determined, n.o.: not observed; [e)]Between-subject effects of treatment, analysis of variance (ANOVA), $p < 0.05$; [f)]G10_LNCO3 different from G10_LNCO8, unpaired t-test $p < 0.05$.

walls of G10_LNCO8 compared to G10_LNCO3. However, no differentiation occurred during the first nine days of culture. The use of an osteoinductive cell culture medium induced differentiation into the osteogenic lineage, with a larger number of cells differentiated on G10_LNCO3. This indicated that a material with a higher local modulus allows for preferential osteogenic differentiation of hMSCs. In an in vivo situation, protein adsorption is a process occurring immediately after implantation. Protein adsorption was exemplarily investigated by incubating the ArcGels with fibronectin, which interacts strongly with gelatin, prior to the cell settling. The fibronectin enhanced the viability as well as the differentiation of the hMSCs. A possible rationale is that fibronectin offers additional sites of adhesion for the cells.

The capacity to induce bone regeneration of the two ArcGels was assessed by implantation ($n = 6$ each) into 5 mm (critical size) mid-diaphyseal femoral defects in female Sprague Dawley rats (weight at operation: 250–300 g) (Figure 5b and Figure S7, Supporting Information). The defects were stabilized by an external unilateral fixator.[25] As control, cancellous bone grafts were used to compare the healing capacity of the ArcGels against a clinically relevant defect treatment strategy ($n = 5$).[10] All animal experiments were carried out according to the policies and procedures approved by the local legal representative (LAGeSo Berlin, G0210/08). Bone healing was quantified at six weeks postoperation using microcomputed tomography (Figure 5c and **Table 1**). An independent-group *t*-test was performed (SAS 9.1; SAS Institute, Inc., Cary, NC). The total callus volume, mineralized callus volume, and tissue mineral content were significantly greater in the G10_LNCO3 compared to the G10_LNCO8 after six weeks postoperation ($p < 0.044$). Therefore, the data indicated that the G10_LNCO3 ArcGel showed enhanced bone defect healing compared to the G10_LNCO8.

In summary, G10_LNCO3 had a comparable healing capacity (total callus volume, mineralized callus volume, and tissue mineral content) to that of the clinical standard, cancellous bone graft. In an initial step, homing of host cells is enabled by the ArcGels. It can be suggested that local mechanical properties in an interconnected porous hydrogel together with the stress through pore growth during the degradation phase appear to guide endogenous stroma cell behavior, and that such step appears important to initiate the healing cascade found in endogenous regeneration. It is remarkable that a rapidly degrading material can induce such an osteoinductive effect. These findings demonstrate that a biomaterial with appropriate micromechanical properties together with dynamic changes during the degradation can guide the in vivo bone regeneration under clinically challenging healing conditions. ArcGels are an example for a knowledge-based design of a multifunctional material, whereby the functions are associated to different hierarchical levels. The introduced biopolymer-based implant system does not require external preloading with cells or simultaneous application of bioactive growth factors. The single step synthesis and formation process of ArcGels, whose micromechanical properties and degradation behavior can be adjusted by only small changes in their chemistry, makes their translation realistic.

Supporting Information

Supporting Information is available from the Wiley Online Library or from the author.

Acknowledgements

The authors thank the Deutsche Forschungsgemeinschaft (DFG) for partially funding this work through SFB 760 subprojects B5 and C2, and the Helmholtz Association for partial funding through the Berlin–Brandenburg Center for Regenerative Therapies, Grant No. SO-036.

Received: October 16, 2014
Revised: December 15, 2014
Published online: January 20, 2015

[1] P. P. Spicer, J. D. Kretlow, S. Young, J. A. Jansen, F. K. Kasper, A. G. Mikos, *Nat. Protoc.* **2012**, *7*, 1918.
[2] J. C. Reichert, S. Saifzadeh, M. E. Wullschleger, D. R. Epari, M. A. Schütz, G. N. Duda, H. Schell, M. van Griensven, H. Redl, D. W. Hutmacher, *Biomaterials* **2009**, *30*, 2149.
[3] a) Anonymous, *WHO Tech. Rep. Ser.* **2003**, *919*, 1; b) D. Heinegård, L. Lidgren, T. Saxne, *Bull. World Health Org.* **2003**, *81*, 686.
[4] a) I. Arrighi, S. Mark, M. Alvisi, R. B. von, J. A. Hubbell, J. C. Schense, *Biomaterials* **2009**, *30*, 1763; b) R. C. de Guzman, J. M. Saul, M. D. Ellenburg, M. R. Merrill, H. B. Coan, T. L. Smith, M. E. Van Dyke, *Biomaterials* **2013**, *34*, 1644; c) U. Ripamonti, *Biomaterials* **2006**, *27*, 807; d) J.-H. Ye, Y.-J. Xu, J. Gao, S.-G. Yan, J. Zhao, Q. Tu, J. Zhang, X.-J. Duan, C. A. Sommer, G. Mostoslavsky, D. L. Kaplan, Y.-N. Wu, C.-P. Zhang, L. Wang, J. Chen, *Biomaterials* **2011**, *32*, 5065.
[5] a) L. L. Hench, J. M. Polak, *Science* **2002**, *295*, 1014; b) M. P. Lutolf, G. P. Raeher, A. H. Zisch, N. Tirelli, J. A. Hubbell, *Adv. Mater.* **2003**, *15*, 888.
[6] a) R. Langer, J. P. Vacanti, *Science* **1993**, *260*, 920; b) R. Quarto, M. Mastrogiacomo, R. Cancedda, S. M. Kutepov, S. Mukhachev, A. Lavroukov, E. Kon, M. Marcacci, *N. Engl. J. Med.* **2001**, *344*, 385.

[7] a) H. Petite, V. Viateau, W. Bensaid, A. Meunier, C. de Pollak, M. Bourguignon, K. Oudina, L. Sedel, G. Guillermin, *Nat. Biotechnol.* **2000**, *18*, 959; b) L. L. Hench, *Science* **1980**, *208*, 826; c) M. Mastrogiacomo, A. Papadimitropoulos, A. Cedola, F. Peyrin, P. Giannoni, S. G. Pearce, M. Alini, C. Giannini, A. Guagliardi, R. Cancedda, *Biomaterials* **2007**, *28*, 1376; d) J. Tu, H. Wang, H. Li, K. Dai, J. Wang, X. Zhang, *Biomaterials* **2009**, *30*, 4369; e) D. Zou, Z. Zhang, J. He, S. Zhu, S. Wang, W. Zhang, J. Zhou, Y. Xu, Y. Huang, Y. Wang, W. Han, Y. Zhou, S. Wang, S. You, X. Jiang, Y. Huang, *Biomaterials* **2011**, *32*, 9707; f) B. Levi, A. W. James, E. R. Nelson, D. Vistnes, B. Wu, M. Lee, A. Gupta, M. T. Longaker, *PLoS ONE* **2010**, *5*, e11177.
[8] I. K. Ko, S. J. Lee, A. Atala, J. J. Yoo, *Exp. Mol. Med.* **2013**, *45*, e57.
[9] a) H. Huang, X. Zhang, X. Hu, Z. Shao, J. Zhu, L. Dai, Z. Man, L. Yuan, H. Chen, C. Zhou, Y. Ao, *Biomaterials* **2014**, *35*, 9608; b) C. H. Lee, J. L. Cook, A. Mendelson, E. K. Moioli, H. Yao, J. J. Mao, *Lancet* **2010**, *376*, 440.
[10] C. G. Finkemeier, *J. Bone Jt. Surg.* **2002**, *84A*, 454.
[11] a) C. Myeroff, M. Archdeacon, *J. Bone Jt. Surg.* **2011**, *93*, 2227; b) H. M. Heneghan, J. P. McCabe, *BMC Musculoskelet. Disord.* **2009**, *10*, 158.
[12] L. Claes, S. Recknagel, A. Ignatius, *Nat. Rev. Rheumatol.* **2012**, *8*, 133.
[13] T. Rozario, D. W. DeSimone, *Dev. Biol.* **2010**, *341*, 126.
[14] J. Elisseeff, *Nat. Mater.* **2008**, *7*, 271.
[15] a) N. Huebsch, P. R. Arany, A. S. Mao, D. Shvartsman, O. A. Ali, S. A. Bencherif, J. Rivera-Feliciano, D. J. Mooney, *Nat. Mater.* **2010**, *9*, 518; b) K. Chatterjee, S. Lin-Gibson, W. E. Wallace, S. H. Parekh, Y. Jong Lee, M. T. Cicerone, M. F. Young, C. G. Simon Jr., *Biomaterials* **2010**, *31*, 5051.
[16] a) A. J. Engler, S. Sen, H. L. Sweeney, D. E. Discher, *Cell* **2006**, *126*, 677; b) M. P. Lutolf, P. M. Gilbert, H. M. Blau, *Nature* **2009**, *426*, 433; c) P. M. Gilbert, K. L. Havenstrite, K. E. G. Magnusson, A. Sacco, N. A. Leonardi, P. Kraft, N. K. Nguyen, S. Thrun, M. P. Lutolf, H. M. Blau, *Science* **2010**, *329*, 1078.
[17] T. Dvir, B. P. Timko, D. S. Kohane, R. Langer, *Nat. Nanotechnol.* **2011**, *6*, 13.
[18] a) K. W. Lee, S. Wang, M. J. Yaszemski, L. Lu, *Biomaterials* **2010**, *29*, 2839; b) F. J. O'Brien, B. A. Harley, I. V. Yannas, L. J. Gibson, *Biomaterials* **2005**, *26*, 433.
[19] C. M. Murphy, M. G. Haugh, F. J. O'Brien, *Biomaterials* **2010**, *31*, 461.
[20] E. S. Place, N. D. Evans, M. S. Stevens, *Nat. Mater.* **2009**, *8*, 457.
[21] K. M. Hennessy, B. E. Pollot, W. C. Clem, M. C. Phipps, A. A. Sawyer, B. K. Culpepper, S. L. Bellis, *Biomaterials* **2009**, *30*, 1898.
[22] G. Tronci, A. T. Neffe, B. F. Pierce, A. Lendlein, *J. Mater. Chem.* **2010**, *20*, 8875.
[23] M. Behl, A. Lendlein, *Soft Matter* **2007**, *3*, 58.
[24] D. W. Hutmacher, *J. Biomater. Sci., Polym. Ed.* **2001**, *12*, 107.
[25] M. Mehta, H. Schell, C. Schwarz, A. Peters, K. Schmidt-Bleek, A. Ellinghaus, *Arch. Orthop. Trauma Surg.* **2011**, *131*, 121.
[26] Measurements in the SEM are subject to methodological and statistical errors due to the sample preparation (drying, cutting, breakline, angle to the observer) and nonstatistical choice of data points.